Contrib Mineral Petrol (2012) 163:689–700
DOI 10.1007/s00410-011-0693-5

ORIGINAL PAPER

The effect of chemical composition and oxygen fugacity on the electrical conductivity of dry and hydrous garnet at high temperatures and pressures

Lidong Dai · Heping Li · Haiying Hu · Shuangming Shan · Jianjun Jiang · Keshi Hui

Received: 15 April 2011 / Accepted: 5 September 2011 / Published online: 21 September 2011

Abstract The in situ electrical conductivity of hydrous garnet samples ($Py_{20}Alm_{76}Grs_4$–$Py_{73}Alm_{14}Grs_{13}$) was determined at pressures of 1.0–4.0 GPa and temperatures of 873–1273 K in the YJ-3000t apparatus using a Solartron-1260 impedance/gain-phase analyzer for various chemical compositions and oxygen fugacities. The oxygen fugacity was controlled by five solid-state oxygen buffers ($Fe_2O_3 + Fe_3O_4$, Ni + NiO, Fe + Fe_3O_4, Fe + FeO, and Mo + MoO_2). Experimental results indicate that within a frequency range from 10^{-2} to 10^6 Hz, electrical conductivity is strongly dependent on signal frequency. Electrical conductivity shows an Arrhenius increase with temperature. At 2.0 GPa, the electrical conductivity of anhydrous garnet single crystals with various chemical compositions ($Py_{20}Alm_{76}Grs_4$, $Py_{30}Alm_{67}Grs_3$, $Py_{56}Alm_{43}Grs_1$, and $Py_{73}Alm_{14}Grs_{13}$) decreases with increasing pyrope component (Py). With increasing oxygen fugacity, the electrical conductivity of dry $Py_{73}Alm_{14}Grs_{13}$ garnet single crystal shows an increase, whereas that of a hydrous sample with 465 ppm water shows a decrease, both following a power law (exponents of 0.061 and −0.071, respectively). With increasing pressure, the electrical conductivity of this hydrous garnet increases, along with the pre-exponential factors, and the activation energy and activation volume of hydrous samples are 0.7731 ± 0.0041 eV and −1.4 ± 0.15 cm^3/mol, respectively. The results show that small hopping polarons $\left(Fe_{Mg}^{\cdot}\right)$ and protons ($H^{\cdot}$) are the dominant conduction mechanisms for dry and wet garnet single crystals, respectively. Based on these results and the effective medium theory, we established the electrical conductivity of an eclogite model with different mineral contents at high temperatures and high pressures, thereby providing constraints on the inversion of field magnetotelluric sounding results in future studies.

Keywords Oxygen fugacity · Chemical composition · Electrical conductivity · Garnet · High temperature and high pressure

Communicated by H. Keppler.

L. Dai · H. Li (✉) · H. Hu · S. Shan · J. Jiang · K. Hui
Laboratory for Study of the Earth's Interior and Geofluids, Institute of Geochemistry, Chinese Academy of Sciences, Guiyang 550002, Guizhou, China
e-mail: hepingli_2007@hotmail.com

L. Dai
Department of Earth and Planetary Sciences, Tokyo Institute of Technology, 2-12-1 Ookayama, Meguro, Tokyo 152-8551, Japan

H. Hu · J. Jiang · K. Hui
Graduate School of Chinese Academy of Sciences, Beijing 100039, China

Introduction

The electrical conductivity of minerals and rocks at relevant temperatures and pressures provides information on the physical and chemical conditions of the Earth's interior, as well as that of other planets. Precise data of electrical conductivity are essential for interpreting the field results obtained by geomagnetic depth sounding and magnetotellurics. Electrical conductivity data obtained in the laboratory provide constraints on the mineralogy, chemical composition, thermal structure, thermodynamic state, water distribution, and partial melting of the Earth's interior (Laštovičková 1991; Roberts and Duba 1995; Xu et al. 1998; Zhang et al. 2006, 2010; Poe et al. 2010;

Pommier et al. 2010; Wu et al. 2010; Ni et al. 2011a, b; Yang et al. 2011a, b).

Garnet is a major rock-forming mineral that is stable over a wide range of pressures and temperatures, from the Earth's crust to the lower mantle. Garnet occurs not only in mantle peridotites but also in eclogite—the high-pressure equivalent of basalt in subducted oceanic crust. Garnet typically contains 80% pyrope-rich garnet in the utramafic rocks of peridotite xenoliths, while it is rich in the almandine and grossular components with several percent of the uvarovite component (MacGregor and Carter 1970; Lu and Keppler 1997; Jin et al. 2001). Garnets from eclogite xenoliths are usually also pyrope-rich, but more variable in their chemical composition (Boyd and Meyer 1979; Lu and Keppler 1997). Deep in the Earth's interior (depths of 300–500 km), pyroxenes are progressively broken down to produce majoritic garnet (Irifune and Ringwood 1993). Previous studies have examined the electrical conductivity of minerals such as olivine, orthopyroxene, clinopyroxene, wadsleyite, and ringwoodite, which only occur within a limited depth range from the upper mantle to the mantle transition zone of the Earth's interior (Xu et al. 1998; Wang et al. 2006; Huang et al. 2005; Dai and Karato 2009a, b; Yang et al. 2011a, b). In contrast, garnet is stable across a broad depth range; consequently, the electrical properties of garnet are important in interpreting geophysical data.

The electrical properties of minerals and rocks are influenced mainly by temperature, pressure, oxygen fugacity, water content, grain boundary state, point-defect chemistry, chemical composition, the distribution of partial melting, and electronic spin-state transitions (Roberts and Tyburczy 1993; Lin et al. 2007; Dai et al. 2008a, b, 2010; Gaillard et al. 2008; Ohta et al. 2008; Farla et al. 2010; Watson et al. 2010). Oxygen fugacity not only drives redox reactions, element partitioning, and structural phase transitions, but also controls certain transport electrical properties and rheological properties, especially in minerals such as silicates and oxides in which oxygen vacancies play a major role in these processes. Previous measurements of the electrical conductivity of garnet only considered the effect of chemical composition or water content (Romano et al. 2006; Dai and Karato 2009c). Recently, a novel technique has been established to control oxygen fugacity during high-pressure conductivity measurements using the Kawai-1000t multi-anvil apparatus at Yale University (USA) and using the YJ-3000t equipment at the Institute of Geochemistry, Chinese Academy of Sciences, Guiyang, China (Dai et al. 2009; Dai and Karato 2009a).

In this study, we determined the electrical conductivity of garnet under various conditions of temperature, pressure, oxygen fugacity, and chemical composition within the frequency range from 10^{-2} to 10^{6} Hz. Five typical oxygen buffers ($Fe_2O_3 + Fe_3O_4$, $Ni + NiO$, $Fe + Fe_3O_4$, $Fe + FeO$, and $Mo + MoO_2$) were employed to control oxygen fugacity. We modeled the dependences of electrical conductivity and discussed the conduction mechanism and the geophysical implications of the experimental results.

Experimental procedures

Sample preparation

Dry gem-grade garnet single crystals with various chemical compositions were collected from alkaline-rich basalt xenoliths in the Altai region of Xinjiang, China, and from Arizona, USA. Electron microprobe and transmission electron microscope observations indicated that the samples (grain sizes of 10–30 mm) are unaltered and free of oxidation. Their chemical compositions are listed in

Table 1 Chemical composition of sample (wt%)

Oxides	H1104	H1109	H1115	H1118
MgO	5.09	7.28	15.92	20.82
NiO	0.07	0.15	0.13	0.01
Al_2O_3	20.9	21.75	21.23	21.51
SiO2	37.71	39.27	38.56	41.81
CaO	1.32	0.96	0.47	5.13
TiO_2	0.01	0.06	0.03	0.07
Cr_2O_3	0.02	0.31	0.05	3.98
K_2O	0.01	0.12	0.06	0.02
Na_2O	0.16	0.15	0.21	0.03
MnO	0.73	0.59	1.13	0.34
FeO	34.25	29.23	22.15	7.42
Total	100.27	99.87	99.94	101.14
Chemical composition	$Py_{20}Alm_{76}Grs_4$	$Py_{30}Alm_{67}Grs_3$	$Py_{56}Alm_{43}Grs_1$	$Py_{73}Alm_{14}Grs_{13}$

Table 1. Given garnet's rhombic trioctahedron structure (isometric crystal system), anisotropy in electrical conductivity was ignored. Four garnet single-crystal samples with different chemical compositions ($Py_{20}Alm_{76}Grs_4$, $Py_{30}Alm_{67}Grs_3$, $Py_{56}Alm_{43}Grs_1$, and $Py_{73}Alm_{14}Grs_{13}$) were carefully selected by means of electron microprobe analyses at Yale University and at the Institute of Geochemistry, Chinese Academy of Sciences. The results of Fourier transform infrared spectroscopy (FTIR) indicate that the original dry samples contain less than 1 ppm water. At 8.0 GPa and 1573 K, the garnet sample with the composition $Py_{73}Alm_{14}Grs_{13}$ was hot-pressed and sintered to obtain a hydrous product with 465 ppm water. For a detailed description of the synthesis of hydrous garnet, see Mookherjee and Karato (2010). Figure 1 shows the FTIR absorption spectra of both dry and hydrous $Py_{73}Alm14Grs_{13}$ garnet.

Buffer preparation

Control of oxygen fugacity was achieved by employing high-purity powders of common metals and metal oxides; i.e., solid buffer pairs containing Ni, Fe, and Mo, as well as NiO, FeO, Fe_2O_3, Fe_3O_4, and MoO_2 [$Fe_2O_3 + Fe_3O_4$ (MH), Ni + NiO (NNO), Fe + Fe_3O_4 (IM), Fe + FeO (IW), and Mo + MoO_2 (MMO)]. Each pair was mechanically mixed at a 1:1 ratio with respect to the metal component.

Under conditions of pressure (P) = 133 MPa and absolute temperature (T) = 1573 K, and employing argon gas as a pressure medium, solid oxygen buffers were tightly pressed and sintered at the China Iron & Steel Research Institute, Peking, China, and the recovered products were cut and polished by electric spark discharge and erosion to obtain electrode slices and buffer loops. For each solid buffer, oxygen fugacity values are a function of temperature and pressure, as follows (Chou and Eugster 1976; Chou 1978):

$$\text{Log } f_{O_2} = -\frac{\alpha}{T} + \beta + \gamma\frac{(P-1)}{T} \quad (1)$$

where α, β, and γ are constants related to the enthalpy, entropy and volume change of the buffer reaction; T is the absolute temperature; and P is the pressure (atm). Figure 2 shows the oxygen fugacities at a pressure of 2.0 GPa. The oxygen fugacity was varied by changing the metal type in the ring, by using a Faraday shielding cage, and by using buffer electrodes at a given temperature and pressure (Fig. 3). The validity of this approach was assessed by X-ray diffraction analysis after conductivity measurements.

Experimental methods and principles

In situ measurements of high-pressure electrical conductivity were performed using the YJ-3000t multi-anvil press and a Solartron-1260 impedance/gain-phase analyzer at the Laboratory for Study of the Earth's Interior and Geofluids, Institute of Geochemistry, Chinese Academy of Sciences, Guiyang, China. For a detailed description of the apparatus, see Li et al. (1998, 1999) and Xie et al. (2002).

Figure 3 shows the experimental assemblage for measurements of electrical conductivity. High pressures were generated by six tungsten carbide anvils with a total surface area of 23.4 mm^2. Pressure calibration of the sample cell was performed using the melting curves of Cu, Al, Zn, and Pb metals in conjunction with 3D polynomial

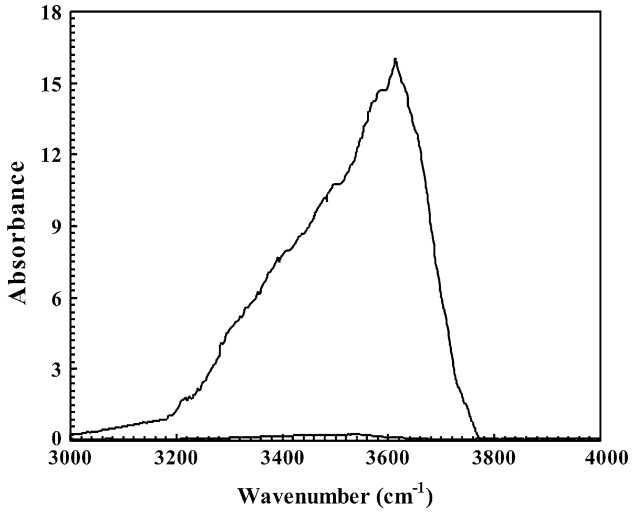

Fig. 1 Fourier transform infrared spectroscopy spectra of hydrous and dry garnet, $Py_{73}Alm_{14}Grs_{13}$. Using the Paterson equation (Paterson 1982), the water content of the hydrous sample was found to be 465 ppm, and that of the anhydrous sample was 0.13 ppm

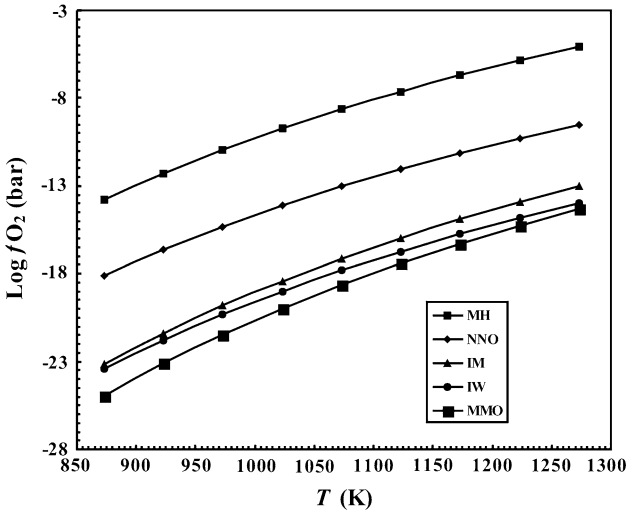

Fig. 2 Dependence of oxygen fugacity, f_{O_2}, on temperature at 2.0 GPa

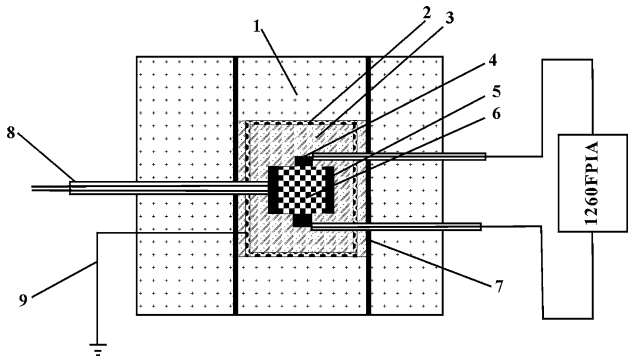

Fig. 3 Experimental setup for electrical conductivity measurements at high pressures and temperatures. *1*: Pyrophyllite; *2*: metal shielding cases; *3*: boron nitride; *4*: electrode; *5*: solid buffer tube; *7*: tri-layer stainless steel heater; *8*: Pt–$Pt_{90}Rh_{10}$ thermocouple; *9*: earth line

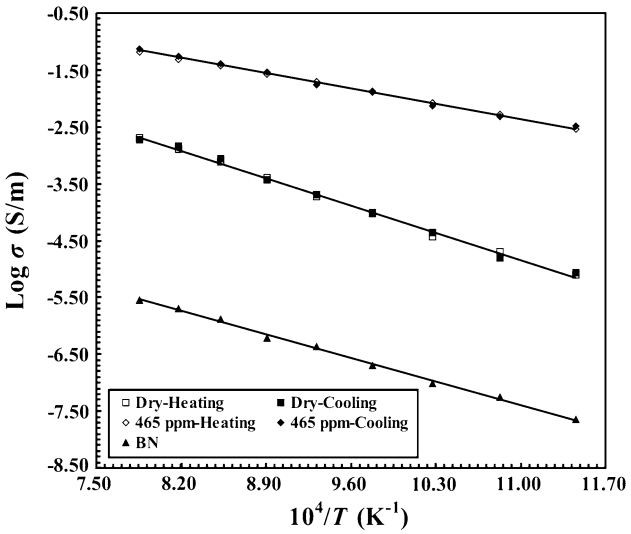

Fig. 4 Electrical conductivity of garnet over a typical heating and cooling cycle at 2.0 GPa. Also shown is the conductivity of boron nitride under the same conditions

numerical fitting under conditions of 1.0–5.0 GPa and 662–1518 K (Shan et al. 2007). Temperature calibration was based on experimental measurements of the elastic wave velocity of plagioclase under conditions of 2.0 GPa and 773–1073 K (Liu et al. 2003). To avoid the influence of absorbed water on the electrical conductivity measurements, the pressure medium of pyrophyllite ($32.5 \times 32.5 \times 32.5$ mm^3) was heated at 923 K for 2 h prior to the experiments. A Faraday shielding case of 0.05-mm metal foil, grounded to Earth, was installed between the pressure medium and the boron nitride (BN) insulation tube to reduce the temperature gradient inside the sample cell, to minimize current leakage across the pressure medium, and to prevent chemical migration between the sample and the pressure medium. A cylindrical sample was placed on the BN insulation tube between the two metal buffer electrodes. Boron nitride provides better insulation than Al_2O_3 (Fuji-ta et al. 2004). Temperature was monitored by a Pt–$Pt_{90}Rh_{10}$ thermocouple. Errors in the temperature and pressure gradients were measured to be less than 10 K and 0.1 GPa, respectively. The uncertainty of impedance was estimated to be less than 5%, and those from was determined to be dimensional variations in the sample, were less than 8%.

Pressure was first raised at a rate of $\sim$1.0 GPa/h to the designated value. Then, under constant pressure, temperature was raised at a rate of $\sim$50 K/min to the designated value. The frequency range and signal voltage were 10^{-2}–10^6 Hz and 1.0 V, respectively. Impedance spectra were acquired at a temperature interval of 50 K. In the case of temperature fluctuations of less than 1 K within 5 min, heat transfer was considered to have reached equilibrium. Attaining equilibrium with the buffer required another 15–20 min. Impedance spectra were fitted from the first high-frequency impedance semicircle using a representative equivalent circuit that comprises a parallel combination of resistor and capacitor. In most cases, the electrical conductivity was determined during the period of decreasing temperature after the maximum temperature had been attained. However, in a few runs, the conductivity was measured during the periods of increasing and decreasing temperature, to assess the hysteresis.

Figure 4 shows the resistance measurements for a single temperature cycle, showing that the results are consistent between the heating and cooling stages. We found no obvious hysteresis, suggesting that the measured conductivity represents a near-equilibrium value under the physical and chemical conditions of each measurement. This result is consistent with the fact that we found no evidence of water loss during the experiments. Water content was determined before and after measurements of the electrical conductivity of the hydrous sample, indicating water loss of less than 10%. To confirm that our results are unaffected by leakage current through the sample and the insulator by BN, we replaced the sample with BN as the background resistivity. The resistivity of a BN disk is $\sim 10^{2.5}$ times higher than that of anhydrous samples and more than $\sim 10^5$ times higher than that of hydrous samples. We conclude that the influence of leakage current was negligible under our experimental conditions.

Experimental results

We measured the electrical conductivity of (1) hydrous garnet single crystals ($Py_{73}Alm_{14}Grs_{13}$) at pressures of 1.0–4.0 GPa and temperatures of 873–1273 K, using an Fe + Fe_3O_4 (IM) oxygen buffer; (2) anhydrous garnets of various compositions (including $Py_{20}Alm_{76}Grs_4$,

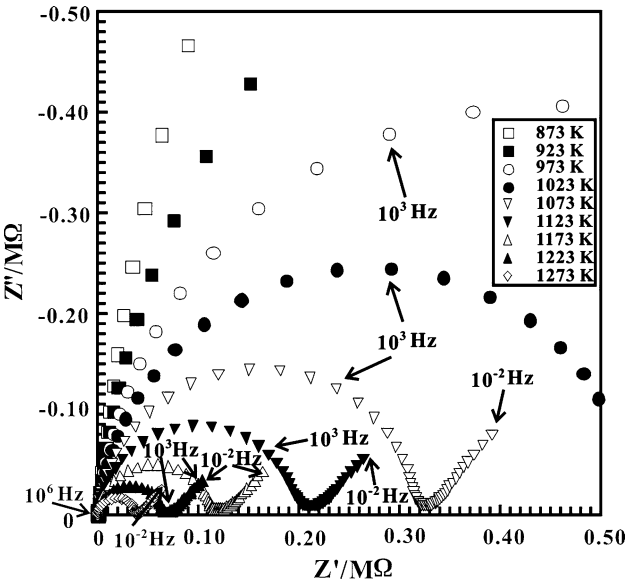

Fig. 5 Nyquist curves of the complex impedance, showing a switch for dry $Py_{30}Alm_{67}Grs_3$ garnet from 10^{-2} to 10^6 Hz (from *right* to *left*), obtained for 2.0 GPa and 873–1273 K with an IM solid buffer. Z′and Z″ denote the real and imaginary components of the complex impedance, respectively

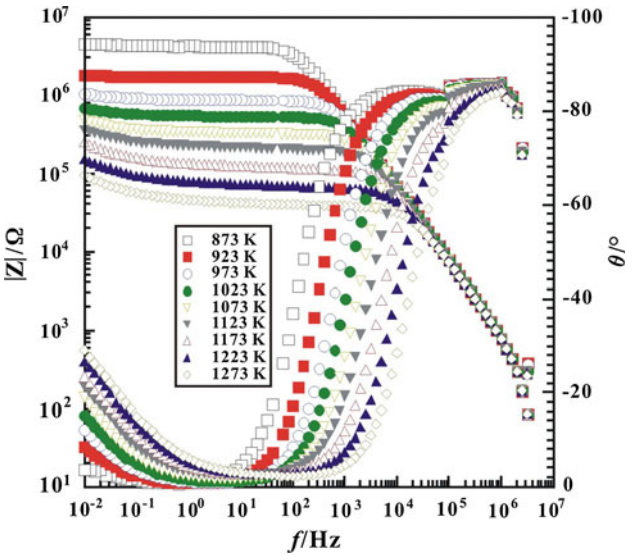

Fig. 6 Dependence of the modulus, $|Z|$, and phase, θ, of the complex impedance of dry $Py_{30}Alm_{67}Grs_3$ garnet on frequency under conditions of 2.0 GPa, 873–1273 K, and with an IM oxygen buffer

$Py_{30}Alm_{67}Grs_3$, $Py_{56}Alm_{43}Grs_1$, and $Py_{73}Alm_{14}Grs_{13}$) using an Fe + Fe_3O_4 (IM) oxygen buffer; and (3) hydrous and anhydrous $Py_{73}Alm_{14}Grs_{13}$, using oxygen buffers of Fe_2O_3 + Fe_3O_4, Ni + NiO, Fe + Fe_3O_4, Fe + FeO, and Mo + MoO_2.

Figures 5 and 6 show representative spectra of a dry garnet single crystal ($Py_{30}Alm_{67}Grs_3$). The spectra in Fig. 5 are in the form of a Nyquist diagram that plots the imaginary part (Z'') against the real part of impedance (Z') at different frequencies (f). Figure 6 is a Bode diagram that depicts the dependence of modulus ($|Z|$) and phase angle (θ) on frequency (f). According to the theory of impedance spectroscopy (Huebner and Dillenburg 1995; Barkmann and Cemič 1996; Bagdassarov 2011), the observed semicircular arcs of complex impedance in the Nyquist diagram are indicative of two different conduction mechanisms. The semicircle in the high-frequency region ($\sim 10^3$–10^6 Hz) corresponds to the grain interior conduction mechanism, whereas that in the low-frequency portion ($\sim 10^{-2}$–10^3 Hz) corresponds to polarization between the sample and the electrodes. With increasing temperature, the inner semicircle shows a decrease in diameter, indicating enhanced electrical conductivity.

Sample resistance (R) is equivalent to the diameter of the high-frequency arc, which converts to electrical conductivity as follows:

$$\sigma = \frac{L/S}{R} = \frac{L}{RS} \tag{2}$$

where σ is electrical conductivity, L is length of sample, and S is the electrode cross-sectional area. The electrical conductivity of garnet single crystal and temperature was found to satisfy the Arrhenius relation:

$$\sigma = \sigma_0 \exp(-\Delta H/KT) \tag{3}$$

where σ_0 is the pre-exponential factor, ΔH is the activation enthalpy, and R is the Boltzmann constant. The activation enthalpy (ΔH) is dependent on pressure:

$$\Delta H = \Delta U + P \times \Delta V \tag{4}$$

where ΔU is the activation energy and ΔV is the activation volume.

Figure 7 shows the electrical conductivity of a garnet single crystal ($Py_{73}Alm_{14}Grs_{13}$) with 465 ppm water under conditions of 1.0–4.0 GPa and using an Fe + Fe_3O_4 solid buffer. Figure 8 shows electrical conductivity as a function of the chemical composition of garnet ($Py_{20}Alm_{76}Grs_4$, $Py_{30}Alm_{67}Grs_3$, $Py_{56}Alm_{43}Grs_1$, and $Py_{73}Alm_{14}Grs_{13}$) at 2.0 GPa and using an IM solid buffer. The effect of oxygen fugacity on electrical conductivity is shown in Fig. 9, and the fitted parameters of the Arrhenius relation are listed in Table 2.

Discussion

Influence of pressure and chemical composition

With increasing pressure, the electrical conductivity of hydrous garnet increases, the pre-exponential factor slightly increases, and the activation enthalpy decreases

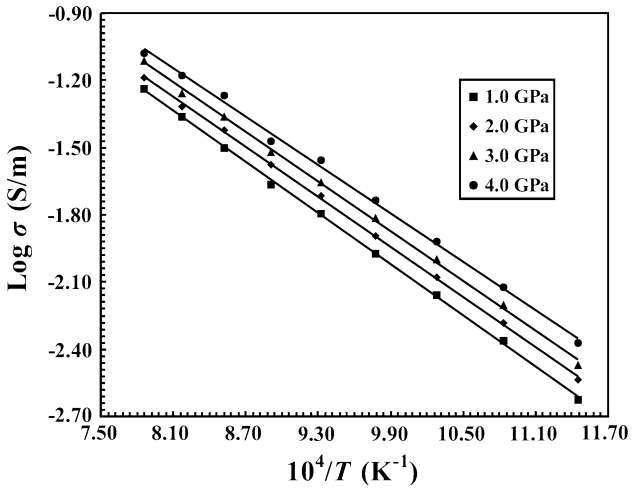

Fig. 7 Logarithm of electrical conductivity versus reciprocal temperature for hydrous $Py_{73}Alm_{14}Grs_{13}$ garnet under conditions of 1.0–4.0 GPa, and with an IM oxygen buffer

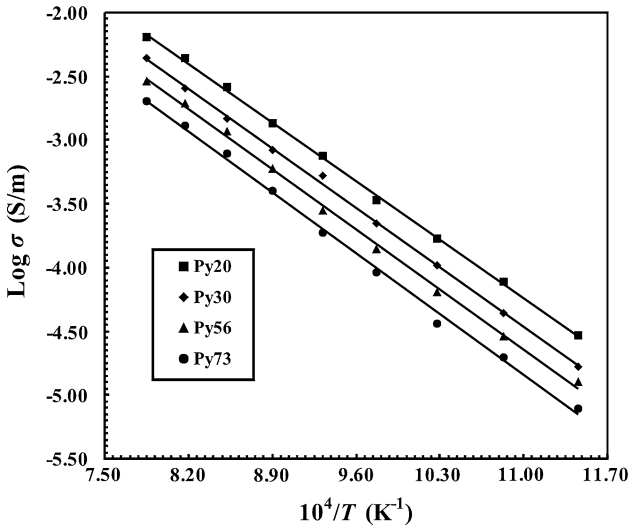

Fig. 8 Electrical conductivity of $Py_{20}Alm_{76}Grs_4$, $Py_{30}Alm_{67}Grs_3$, $Py_{56}Alm_{43}Grs_1$, and $Py_{73}Alm_{14}Grs_{13}$ garnet at 2.0 GPa with an IM oxygen buffer. The *legend* indicates the garnet compositions (mol% pyrope)

(Fig. 7). Although previous studies have examined the electrical conductivity of the (dry) dominant minerals in the upper mantle (e.g., olivine, pyroxene, and garnet) and assessed their pressure dependences (Xu et al. 2000a; Dai et al. 2005, 2009a, c), no study has assessed the influence of pressure on the electrical conductivity of hydrous minerals. According to Eq. 4 and Table 2, we can further obtain the activation energy and activation volume of charge carriers in hydrous garnet under conditions of 1.0–4.0 GPa, 873–1273 K, and an IM buffer, yielding values of 0.7731 ± 0.0041 eV and -1.4 ± 0.15 cm^3/mol, respectively. The present experimental results are in general agreement with the results reported by Katsura et al. (2007) in terms of positive pressure dependence.

At a pressure of 2.0 GPa and with an IM oxygen buffer (Fig. 8), the electrical conductivity of anhydrous garnet single crystals with various chemical compositions ($Py_{20}Alm_{76}Grs_4$, $Py_{30}Alm_{67}Grs_3$, $Py_{56}Alm_{43}Grs_1$, and $Py_{73}Alm_{14}Grs_{13}$) shows a decrease with increasing pyrope content (Py), the pre-exponential factors also decrease, and the activation enthalpies increase. When the Py content (Py/(Py + Alm + Grs)) in samples increases from 20 to 73%, the electrical conductivity is reduced by ~30%. This observation is in agreement with a recent report by Karato (2011) that theoretically predicted a 50% conductivity increase with increasing Py content from 2 to 90%. The present results also showed that the activation enthalpies (ΔH) of dry samples (1.32–1.37 eV) are significantly higher than those of wet $Py_{73}Alm_{14}Grs_{13}$ garnet (0.71–0.76 eV).

Romano et al. (2006) investigated the electrical conductivity of synthetic pyrope ($Mg_3Al_2Si_3O_{12}$)–almandine ($Fe_3Al_2Si_3O_{12}$) samples and found that electrical conductivity decreases by five orders of magnitude from Py_{100} to Alm_{100}. In addition, they obtained activation enthalpies of 0.56–0.68 eV in the low-temperature zone (573–1273 K) and 1.26–2.56 eV in the high-temperature zone (973–1973 K). Although the authors stated that Mössbauer spectroscopy was used to precisely determine the oxidation state of iron, our results indicate that variation by five orders of magnitude is too large. Our explanation of this discrepancy is that the garnets investigated by Romano et al. (2006) contained a large amount of water, which would have produced anomalously high electrical conductivity, especially in the low-temperature region. Romano et al. (2006) measured pyrope–almandine conductivity from Py100 to Py0 and found a much stronger dependence of activation enthalpy on composition in the high-temperature data (pyrope-rich samples), for which we can be more confident that the samples were anhydrous. The conclusion made by Romano et al. (2006) is strongly based on this observation and is consistent with the results of previous studies regarding the effect of Fe/(Fe + Mg) on the activation enthalpy of conduction in both olivine and pyroxene (Cemič et al. 1980; Seifert et al. 1982). It has been demonstrated that the presence of dissolved water can enhance the electrical conductivity of minerals by several orders of magnitude (Huang et al. 2005; Wang et al. 2006; Dai and Karato 2009a, b, c; Yang et al. 2011a, b).

Influence of oxygen fugacity on electrical conductivity

Figure 9 shows the relation between the electrical conductivity of anhydrous and hydrous $Py_{73}Alm_{14}Grs_{13}$ garnet, and oxygen fugacity at 2.0 GPa. As the environment

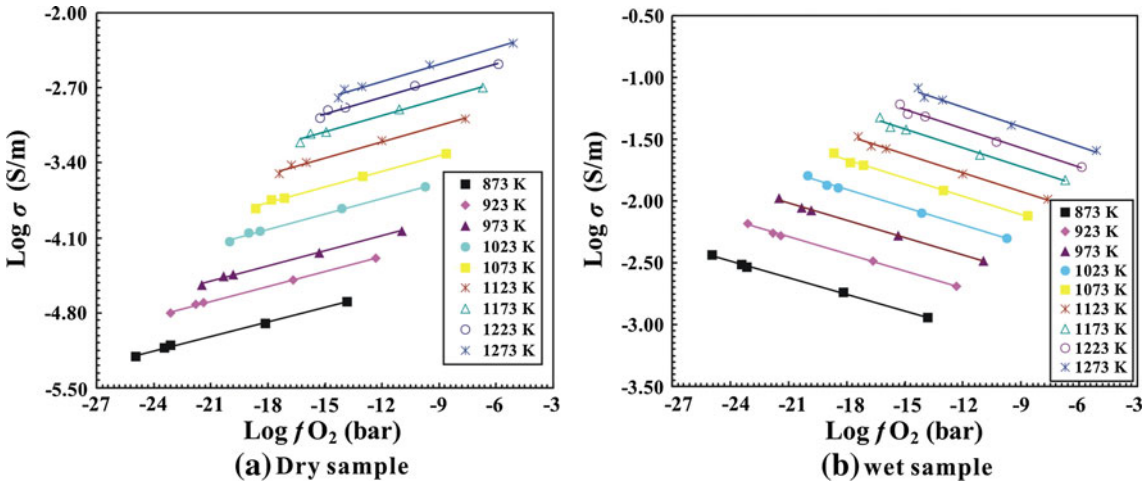

Fig. 9 Electrical conductivity of dry and wet $Py_{73}Alm_{14}Grs_{13}$ garnet for five oxygen buffers ($Fe_2O_3 + Fe_3O_4$, Ni + NiO, Fe + Fe_3O_4, Fe + FeO, and Mo + MoO_2) at 2.0 GPa and 873–1273 K. The water contents of the dry and wet samples are 0.13 and 465 ppm, respectively

Table 2 Fitted parameters of Arrhenius relation for garnet under conditions of 873–1,273 K and IM solid buffer

P (GPa)	Chemical composition	Water content (ppm)	Log σ_0	ΔH (eV)	σ_0 (S m^{-1})	R^2
1.0	$Py_{73}Alm_{14}Grs_{13}$	465	1.7350	0.76	54.33	0.9923
2.0	$Py_{73}Alm_{14}Grs_{13}$	465	1.7422	0.74	55.23	0.9917
3.0	$Py_{73}Alm_{14}Grs_{13}$	465	1.7595	0.73	57.48	0.9952
4.0	$Py_{73}Alm_{14}Grs_{13}$	465	1.7688	0.71	58.72	0.9899
2.0	$Py_{73}Alm_{14}Grs_{13}$	0.18	2.6918	1.37	491.81	0.9956
2.0	$Py_{56}Alm_{43}Grs_{1}$	0.13	2.7740	1.35	594.29	0.9934
2.0	$Py_{30}Alm_{67}Grs_{3}$	0.22	2.8876	1.34	771.97	0.9941
2.0	$Py_{20}Alm_{76}Grs_{4}$	0.16	2.9930	1.32	984.01	0.9915

becomes more oxidized, the electrical conductivity of dry $Py_{73}Alm_{14}Grs_{13}$ garnet increases, whereas the electrical conductivity of the wet sample (465 ppm water) decreases. At 2.0 GPa, the relation between the electrical conductivity of anhydrous and hydrous samples, and oxygen fugacity can be described respectively as:

$$\log_{10}\sigma = (2.23 \pm 0.063) + (0.061 \pm 0.002) \times \log_{10} f_{O_2} + \frac{(-6092 \pm 94)}{T} \quad (5)$$

$$\log_{10}\sigma = (2.27 \pm 0.032) + (-0.071 \pm 0.001) \times \log_{10} f_{O_2} + \frac{(-6475 \pm 48)}{T} \quad (6)$$

The exponential factors of the dependence of the electrical conductivities of the anhydrous and hydrous samples on oxygen fugacity (q) are 0.061 and −0.071, respectively. These values are lower than the results of theoretical calculations performed by Karato (2008a), who developed models for the concentration of point defects in $(Mg,Fe)_2SiO_4$ or $(Mg,Fe)SiO_3$, depending on the chemical environment under chemically neutral conditions for either $[Fe_M^{\cdot}] = [H_M']$ (assuming the sample is anhydrous: $p = 1/4$, $q = 1/8, r = -1/2$; assuming the sample is hydrous: $p = 3/4$, $q = -1/8, r = -1/2$) or $[Fe_M^{\cdot}] = [V_M'']$ (assuming the sample is anhydrous: $p = 0$, $q = 1/6$, $r = -1/3$; assuming the sample is hydrous: $p = 1/2$, $q = -1/12$, $r = -1/3$). The absolute values of q (0.061–0.071) for pyrope-rich garnet are less than predicted, suggesting the involvement of other charge neutrality conditions, such as $[Fe_M^{\cdot}] = [(4H)_{Si}^{\times}]$ and $[Fe_M^{\cdot}] = [(OH)_i']$, or that chemical equilibrium was only partly obtained.

The observed values of q are very close to the exponents (0.05 and −0.058) obtained by Dai and Karato (2009a) for dry and wet wadsleyite, respectively, under conditions of 15 GPa, 873–1273 K, and with three solid-state oxygen buffers (Mo + MoO_2, Ni + NiO, and Re + ReO_2). In addition, the exponent for dry garnet (0.061) is similar to the exponent of 0.096 determined by Dai et al. (2010) for polycrystalline olivine under conditions of 1.0–4.0 GPa, 1073–1423 K, and with five solid-state oxygen buffers ($Fe_2O_3 + Fe_3O_4$, Ni + NiO, Fe + Fe_3O_4, Fe + FeO, and Mo + MoO_2).

According to previous studies on the conduction mechanisms of olivine, orthopyroxene, clinopyroxene, pyrope-rich garnet, wadsleyite, and ringwoodite (Schock and Duba 1985; Xu et al. 1999, 2000a; Huang et al. 2005; Romano et al. 2006; Wang et al. 2006; Dai and Karato 2009a, b, c), lattice point-defect reactions in anhydrous and hydrous garnet samples can be described as follows:

$$Fe^{X}_{Mg} + h^{\cdot} \rightleftharpoons Fe^{\cdot}_{Mg} \quad (7)$$

$$2(H)^{X}_{M} \rightleftharpoons H'_{M} + H^{\cdot} \quad (8)$$

where Fe^{X}_{Mg} is a ferrous ion occupying the magnesium ion site in the lattice structure of the mineral, $h^{\cdot}$ is a hole, $Fe^{\cdot}_{Mg}$ is a trivalent ferric ion at the magnesium ion site in the lattice (i.e., a small polaron), H^{X}_{M} is a hydrogen ion occupying the magnesium or iron ion site, H'_{M} is a hydrogen vacancy at a magnesium or iron ion site, and $H^{\cdot}$ is a hydrogen hole (i.e., a proton).

An increase in oxygen fugacity is accompanied by an increase in the concentrations of point defects according to reaction (7). Because the electrical conductivity of dry garnet shows a positive relation with the concentration of point defects, the electrical conductivity increases with higher oxygen fugacity and a higher concentration of small polarons arising from a point-defect reaction. Oxygen fugacity has the opposite influence on proton conduction, which explains the negative effect of oxygen fugacity on the electrical conductivity of hydrous garnet, as noted by Dai and Karato (2009a).

Geophysical implications

In general, the relation between electrical conductivity and depth in the Earth's interior is established based on the electrical properties of the relevant minerals over a certain depth range. An electrical conductivity-depth profile to depths of 660 km, based on laboratory data of electrical properties and phase transitions in the olivine–wadsleyite–ringwoodite system, shows a conductivity increase of almost two orders of magnitude across the 410-km discontinuity, thereby supporting a double-layer model for the upper mantle (Xu et al. 1998). Recent studies on the electrical conductivity of hydrous wadsleyite (Huang et al. 2005; Dai and Karato 2009a) not only confirmed the hypothesis of hydrogen-enhanced conductivity, but also showed that the earlier results by Xu et al. (1998) were affected by the unrecognized role of hydrogen. The influence of hydrogen is pronounced, and water content in the Pacific transition zone is estimated to be $\sim$0.1–0.2 wt%, which is sufficient to promote partial melting (Huang et al. 2005; Karato 2008b; Karato and Dai 2009; Dai and Karato 2009a).

Despite the fact that garnet is the second abundant mineral in the deep upper mantle and in the transition zone is surpassed in abundance only by olivine–wadsleyite–ringwoodite, few studies have examined its electrical conductivity. Kavner et al. (1995) measured the electrical conductivity of a natural meteoritic majoritic garnet at room pressure and temperatures of 290–370 K, although various assumptions and approximations are required to extrapolate the results to realistic mantle conditions. Xu and Shankland (1999) examined the electrical conductivity of alumina-bearing (2.89 wt%) San Carlos orthopyroxene under conditions of 5–21 GPa and 1273–1673 K. However, the recovered sample was a mixture of garnet and ilmenite. Romano et al. (2006) attempted to construct a conductivity-depth profile according to experimentally derived electrical properties of synthetic garnet with different chemical compositions. However, in the absence of precise analyses of water content by Fourier transform infrared spectroscopy (FTIR) or secondary ion mass spectrometry (SIMS), it is difficult to evaluate the reliability of their data, as noted above.

In this section, our goal is to establish an electrical conductivity model for eclogite based on the laboratory-based conductivity measurements of the present work and previous studies. To simplify the model, we make the following necessary assumptions and extrapolations: (1) the temperatures and pressures are within the ranges 673–1273 K and 0–4.0 GPa, respectively, the upper bounds of which are approximately equivalent to the *P–T* conditions of the base of the lithosphere; (2) oxygen fugacity is employed by a solid buffer Ni + NiO to a value that is very close to that in the upper mantle (Xu et al. 2000b); (3) because the sample is anhydrous, the partitioning coefficient of water among different mineral phases is not considered; (4) the chemical composition of eclogite is constrained to the specific stoichiometry of pyrope-rich garnet with the chemical composition of $Py_{73}Alm_{14}Grs_{13}$; (5) grain boundaries have a negligible influence on the bulk electrical conductivity of the rock; (6) mineral phases are randomly and evenly distributed throughout the eclogite; (7) according to the geochemical classification of eclogite (Mottana et al. 1971), it contains 40–80% pyrope-rich garnet and 20–60% clinopyroxene; secondary minerals are ignored, assuming they have a negligible effect on the bulk electrical conductivity of eclogite; (8) a representative effective medium model is applied to determine the electrical conductivity of eclogite.

Given the above assumptions, the representative bulk electrical conductivity of the eclogite (σ_{EM}) is expressed as follows:

$$\sigma_{EM} = \frac{1}{4}\left\{(3f_{Gt}-1)\sigma_{Gt} + (3f_{CPx}-1)\sigma_{CPx} + \left[\langle(3f_{Gt}-1)\sigma_{Gt} + (3f_{CPx}-1)\sigma_{CPx}\rangle^2 + 8\sigma_{Gt}\sigma_{CPx}\right]^{\frac{1}{2}}\right\} \quad (9)$$

where σ_{Gt} and σ_{CPx} are the electrical conductivities of garnet and clinopyroxene, respectively; and f_{Gt} and f_{CPx} are the volume fractions of garnet and clinopyroxene, respectively. Equation 9 shows that if the electrical conductivities of the constituent phases (garnet and clinopyroxene) are known at a given temperature and pressure, and if the rock has been assigned values of f_{Gt} and f_{CPx}, then the bulk electrical conductivity of the rock is easily determined.

In the present work, we have already obtained experimental results for the electrical conductivity of dry $Py_{73}Alm_{14}Grs_{13}$ garnet under conditions of 2.0 GPa, 873–1273 K, and with a Ni–NiO solid buffer. Under these conditions, there is no phase transition for dry pyrope-rich garnet; therefore, we assume that the Arrhenius behavior at temperatures of 873–1273 K, as described above, may be extended to 873–1473 K on the basis of well-constrained parameters in the Arrhenius equation, such as the pre-exponential factor σ_0 and the activation enthalpy ΔH. To establish the model, we must determine the electrical conductivity of clinopyroxene described by Eq. 9 at high temperatures and pressures. In fact, many previous studies have examined the electrical conductivity of clinopyroxene (Huebner and Voigt 1988; Alekseev and Galanov 1990; Wang et al. 1999; Xu and Shankland 1999; Yang et al. 2011a). Here, we use the electrical conductivity data on clinopyroxene reported by Yang et al. (2011a), mainly because their experimental temperatures and pressures are similar to those of the current work, and because they adopted a measurement technique of alternating current impedance spectroscopy, which is consistent with our measurements of the electrical conductivity of garnet. Anisotropy may influence measurements of the electrical conductivity of clinopyroxene; however, the results obtained for diopside by Dai et al. (2005) indicate that this effect is feeble and can be ignored.

Using Eq. 9, the bulk electrical conductivity of eclogite was calculated under various temperatures and volume ratios of garnet to clinopyroxene (Figs. 10, 11, 12). For comparison, also plotted in Fig. 10 is the electrical conductivity data of natural eclogite, as measured by Laštovičková (1975).

The electrical conductivity of eclogite decreases with increasing garnet content (Fig. 10), although this trend becomes weaker with increasing temperature. Our conductivity results on eclogite are in the good agreement with those of Laštovičková (1975), although a small discrepancy in the lower-temperature region may reflect the different

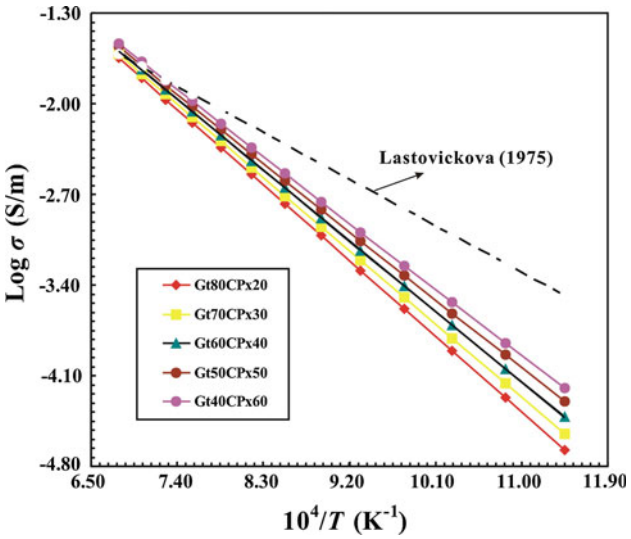

Fig. 10 Logarithm of the calculated electrical conductivity versus reciprocal temperature for eclogite with different volume ratios of garnet to clinopyroxene under conditions of 2.0 GPa, and with a Ni–NiO oxygen buffer. The clinopyroxene data are from Yang et al. (2011a). The dashed line shows the electrical conductivity of eclogite during cooling at room pressure, as reported by Laštovičková (1975)

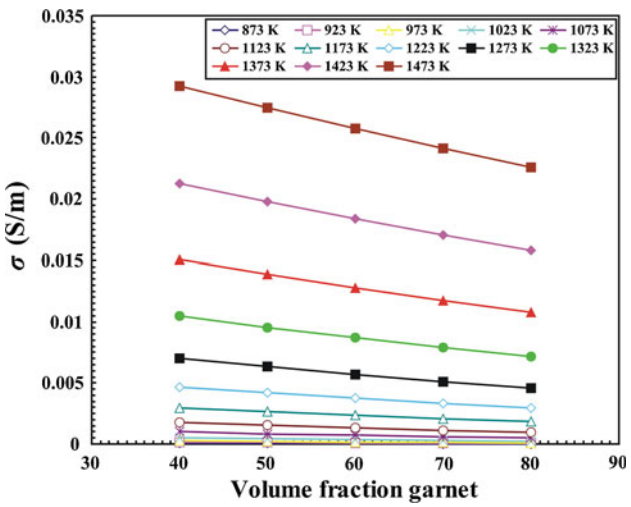

Fig. 11 Effect of garnet fraction on electrical conductivity of eclogite at conditions of 2.0 GPa, 873–1473 K and the Ni–NiO oxygen buffer

mineralogical constituents of the two studies. The natural eclogite sample used by Laštovičková (1975) consisted of garnet (40%), clinopyroxene (45%), quartz (10%), amphibole (2%), rutile (2%), and minor symplectite minerals that include amphibole–plagioclase, diopside–plagioclase, and diopside–magnetite (1%). In the present study, in contrast, the samples consisted of varying volume ratios of garnet and clinopyroxene.

Figure 11 shows the relation between the electrical conductivity of eclogite and volume percentage of garnet

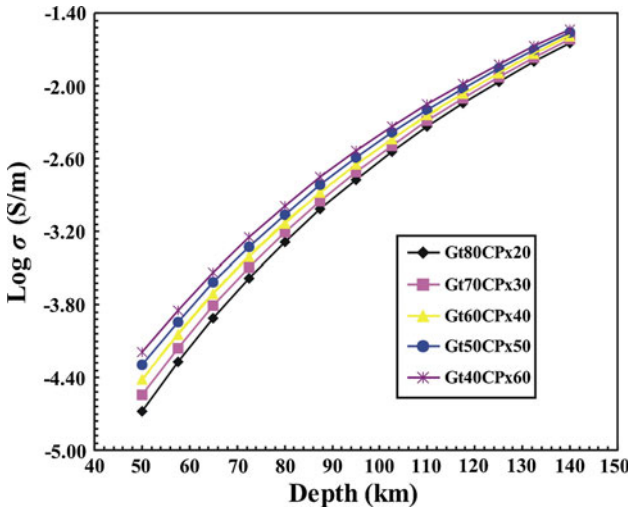

Fig. 12 Laboratory-based conductivity-depth profile on eclogite with different volume ratios garnet to clinopyroxene mineralogical compositions at depth range from 40 to 150 km

under conditions of 2.0 GPa, 873–1473 K, and with a Ni–NiO solid buffer. The bulk electrical conductivity of eclogite shows a linear decrease with increasing volume percentage of garnet, and this relation is strengthened at higher temperatures. Considering the result for clinopyroxene reported by Yang et al. (2011a), we found that the electrical conductivity of garnet is lower than that of clinopyroxene at a given temperature, pressure, and oxygen fugacity. In conclusion, the electrical conductivity of eclogite is affected mainly by garnet content.

Figure 12 shows the logarithm of the electrical conductivity of eclogite with varying mineralogical constituents at temperatures of 873–1473 K, and with a Ni–NiO solid buffer, at depths of 40–150 km. To establish the depth profile of the electrical conductivity of eclogite, we adopt a relatively gentle geothermal gradient of ~6.67°C/km in the pyrolite model (Basu et al. 1986). Figure 12 shows that (1) the logarithmic electrical conductivity of eclogite with various volume ratios of garnet to clinopyroxene shows a smooth increase with increasing depth; (2) the rate of change of electrical conductivity with depth becomes smaller with increasing depth; and (3) the electrical conductivity of eclogite increases with increasing volume percentage of clinopyroxene at constant temperature and pressure. Therefore, a depth profile of the laboratory-based conductivity of eclogite is successfully obtained on the basis of the electrical conductivity of garnet at depths of 40–150 km.

In summary, based on our experimental results for garnet and a model constructed using effective medium theory, we calculated the bulk electrical conductivity of eclogite with various mineralogical compositions under controlled oxygen fugacity and water (hydrogen) content for a broad range of temperatures, pressures, and depths. The results are expected to provide constraints on the inversion of field magnetotelluric (MT) sounding results in future studies.

Acknowledgments We thank two anonymous reviewers and editor of Hans Keppler for their very constructive comments and suggestions in the reviewing process, which helped us greatly in improving the manuscript. The enlightening discussions were conducted with Professor Shun-ichiro Karato (Department of Geology and Geophysics, Yale University, USA) and Dr Huaiwei Ni (Bayerisches Geoinstitut, Universität Bayreuth, Germany). Dr Maniak Mookherjee, Zhicheng Jing, and Zhenting Jiang in Karato's high-pressure laboratory kindly provided technical guidance and assistance. We appreciate Dr Aaron Stallard in Stallard Scientific Editing Company for their helps in English improvements of the manuscript. This research was financially supported by the Knowledge-Innovation Key Orientation Project of CAS (Grant Nos. KZCX2-YW-Q08-3-4 and KZCX2-YW-QN110) and by NSF of China (Grant Nos. 41174079 and 40974051).

References

Alekseev YI, Galanov YI (1990) Electrical conductivity of diopside ceramics. Glass Ceram 47:24–26

Bagdassarov N (2011) Phase transitions in $CsHSO_4$ up to 2.5 GPa: impedance spectroscopy under pressure. J Phys Chem Solids 72:236–244

Barkmann T, Cemič L (1996) Impedance spectroscopy and defect chemistry of fayalite. Phys Chem Miner 23:186–192

Basu AR, Ongley JS, MacGregor ID (1986) Eclogites, pyroxene geotherm, and layered mantle convection. Science 233:1303–1305

Boyd FR, Meyer HOA (eds) (1979) The mantle sample: inclusions in kimberlites and other volcanics. Am Geophys Union, Washington

Cemič L, Will G, Hinze E (1980) Electrical conductivity measurements on olivines Mg_2SiO_4-Fe_2SiO_4 under defined thermodynamic conditions. Phys Chem Miner 6:95–107

Chou IM (1978) Calibration of oxygen buffers at elevated P and T using the hydrogen fugacity sensor. Am Miner 63:690–703

Chou IM, Eugster HP (1976) Fugacity control and dissociation constants of HBr and HI. Contrib Miner Petrol 56:77–100

Dai L, Karato SI (2009a) Electrical conductivity of wadsleyite at high temperatures and high pressures. Earth Planet Sci Lett 287:277–283

Dai L, Karato SI (2009b) Electrical conductivity of orthopyroxene: implications for the water content of the asthenosphere. Proc Jpn Acad Ser B 85:466–475

Dai L, Karato SI (2009c) Electrical conductivity of pyrope-rich garnet at high temperature and high pressure. Phys Earth Planet Int 176:83–88

Dai L, Li H, Liu C, Su G, Cui T (2005) In situ control of oxygen fugacity experimental study on the crystallographic anisotropy of the electrical conductivities of diopside at high temperature and high pressure. Acta Petrol Sin 21:1737–1742

Dai L, Li H, Hu H, Shan S (2008a) Experimental study of grain boundary electrical conductivities of dry synthetic peridotite under high–temperature, high–pressure, and different oxygen fugacity conditions. J Geophys Res 113:B12211. doi:10.1029/2008JB005820

Dai L, Li H, Deng H, Liu C, Su G, Shan S, Zhang L, Wang R (2008b) In situ control of different oxygen fugacity experimental study on the electrical conductivity of lherzolite at high temperature and high pressure. J Phys Chem Solids 69:101–110

Dai L, Li H, Hu H, Shan S (2009) Novel technique to control oxygen fugacity during high-pressure measurements of grain boundary conductivities of rocks. Rev Sci Instrum 80:033903. doi: 10.1063/1.3097882

Dai L, Li H, Li C, Hu H, Shan S (2010) The electrical conductivity of dry polycrystalline olivine compacts at high temperatures and pressures. Miner Mag 74:849–857

Farla RJM, Peach CJ, ten Grotenhuis SM (2010) Electrical conductivity of synthetic iron-bearing olivine. Phys Chem Miner 37:167–178

Fuji-ta K, Katsura T, Tainosho Y (2004) Electrical conductivity measurement of granulite under mid- to lower crustal pressure–temperature conditions. Geophys J Int 157:79–86

Gaillard F, Malki M, Iacono-Marziano G, Pichavant M, Scaillet B (2008) Carbonatite melts and electrical conductivity in the asthenosphere. Science 322:1363–1365

Huang X, Xu Y, Karato SI (2005) Water content of the mantle transition zone from the electrical conductivity of wadsleyite and ringwoodite. Nature 434:746–749

Huebner JS, Dillenburg RG (1995) Impedance spectra of dry silicate minerals and rock: qualitative interpretation of spectra. Am Miner 80:46–64

Huebner JS, Voigt DE (1988) Electrical conductivity of diopside: evidence for oxygen vacancies. Am Miner 73:1235–1254

Irifune T, Ringwood AE (1993) Phase transformations in subducted oceanic crust and buoyancy relationships at depths of 600–800 km in the mantle. Earth Planet Sci Lett 117:101–110

Jin Z, Zhang J, Green HW, Jin SY (2001) Eclogite rheology: implications for subducted lithosphere. Geology 29:667–670

Karato SI (2008a) Deformation of earth materials: introduction to the rheology of the solid earth. Cambridge University Press, Cambridge

Karato SI (2008b) Recent progress in the experimental studies on the kinetic properties in minerals. Phys Earth Planet Inter 170:152–155

Karato SI (2011) Water distribution across the mantle transition zone and its implications for global material circulation. Earth Planet Sci Lett 301:413–423

Karato SI, Dai L (2009) Comments on "Electrical conductivity of wadsleyite as a function of temperature and water content" by Manthilake et al. Phys Earth Planet Inter 174:19–21

Katsura T, Yokoshi S, Kawabe K, Shatskiy A, Okube M, Fukui H, Ito E, Nozawa A, Funakoshi K (2007) Pressure dependence of electrical conductivity of (Mg, Fe)SiO3 ilmenite. Phys Chem Miner 34:249–255

Kavner A, Li X, Jeanloz R (1995) Electrical conductivity of a natural (Mg, Fe)SiO3 majorite garnet. Geophys Res Lett 22:3103–3106

Laštovičková M (1975) The electrical conductivity of eclogites measured by two methods. Studia Geoph Et Geod 19:394–398

Laštovičková M (1991) A review of laboratory measurements of the electrical conductivity of rocks and minerals. Phys Earth Planet Inter 66:1–11

Li H, Xie H, Guo J, Zhang Y, Xu Z, Xu J (1998) In situ control of oxygen fugacity at high temperature and high pressure: a Ni-O system. Geophys Res Lett 25:817–820

Li H, Xie H, Guo J, Zhang Y, Xu Z, Liu C (1999) In situ control of oxygen fugacity at high temperature and high pressure. J Geophys Res 104:29439–29451

Lin JF, Weir ST, Jackson DD, Evans WJ, Vohra YK, Qiu W, Yoo C-S (2007) Electrical conductivity of the lower-mantle ferropericlase across the electronic spin transition. Geophys Res Lett 34:L16305. doi:10.1029/2007GL030523

Liu W, Du J, Yu Y, Bai L, Wang C (2003) Correction of temperature gradient in sample cell of pulse transmission experimental setup on multi-anvil high pressure apparatus. Chin J High Press Phys 17:95–100

Lu R, Keppler H (1997) Water solubility in pyrope to 100 kbar. Contrib Miner Petrol 129:35–42

MacGregor ID, Carter JL (1970) The chemistry of clinopyroxenes and garnets of eclogite and peridotite xenoliths from the Roberts victor mine, South Africa. Phys Earth Planet Inter 3:391–397

Mookherjee M, Karato SI (2010) Solubility of water in pyrope-rich garnet at high pressures and temperature. Geophys Res Lett 37:L03310. doi:10.1029/2009GL041289

Mottana A, Sutterlin PG, May RW (1971) Factor analysis of omphacites and garnets: a contribution to the geochemical classification of eclogites. Contrib Miner Petrol 31:238–250

Ni H, Keppler H, Manthilake M, Katsura T (2011a) Electrical conductivity of dry and hydrous $NaAlSi_3O_8$ glasses and liquids at high pressures. Contrib Miner Petrol 162:501–513

Ni H, Keppler H, Behrens H (2011b) Electrical conductivity of hydrous basaltic melts: implications for partial melting in the upper mantle. Contrib Miner Petrol 162:637–650

Ohta K, Onoda S, Hirose K, Sinmyo R, Shimizu K, Sata N, Ohishi Y, Yasuhara A (2008) The electrical conductivity of post-perovskite in earth's D layer. Science 320:89–91

Paterson MS (1982) The determination of hydroxyl by infrared absorption in quartz, silicate glasses and similar materials. Bull Miner 105:20–29

Poe BT, Romano C, Nestola F, Smyth J (2010) Electrical conductivity anisotropy of dry and hydrous olivine at 8 GPa. Phys Earth Planet Inter 181:103–111

Pommier A, Gaillard F, Pichavant M (2010) Time-dependent changes of the electrical conductivity of basaltic melts with redox state. Geochim Cosmochim Acta 74:1653–1671

Roberts JJ, Duba AG (1995) Transient electrical response of San Quintin dunite as a function of oxygen fugacity changes: information about charge carriers. Geophys Res Lett 22:453–456

Roberts JJ, Tyburczy JA (1993) Impedance spectroscopy of single and polycrystalline olivine: evidence for grain boundary transport. Phys Chem Miner 20:19–26

Romano C, Poe B, Kreidie N, McCammon A (2006) Electrical conductivities of pyrope-almandine garnets up to 19 GPa and 1,700°C. Am Miner 91:1371–1377

Schock RN, Duba A (1985) Point defects and the mechanisms of electrical conduction in olivine. In: Schock RN (ed) Point defects in minerals. American Geophysical Union, Washington, pp 88–96

Seifert KF, Will G, Voigt R (1982) Electrical conductivity measurements on synthetic pyroxenes $MgSiO_3$-$FeSiO_3$ at high pressures and temperatures under defined thermodynamic conditions. In: Schreyer W (ed) High-pressure researches in geoscience. Schweizerbart'sche, Stuttgart, pp 419–432

Shan S, Wang R, Guo J, Li H (2007) Pressure calibration for the sample cell of YJ-3000t multi-anvil press at high-temperature and high-pressure. Chin J High Press Phys 21:367–372

Wang Z, Ji S, Dresen G (1999) Hydrogen-enhanced electrical conductivity of diopside crystals. Geophys Res Lett 26:799–802

Wang D, Mookherjee M, Xu Y, Karato SI (2006) The effect of water on the electrical conductivity of olivine. Nature 443:977–980

Watson HC, Roberts JJ, Tyburczy JA (2010) Effect of conductive impurities on electrical conductivity in polycrystalline olivine. Geophys Res Lett 37:L02302. doi:10.1029/2009GL041566

Wu X, Zhang B, Xu J, Katsura T, Zhai S, Yoshino T, Manthilake G, Shatskiy A (2010) Electrical conductivity measurements of periclase under high pressure and high temperature. Phys B 405:53–56

Xie H, Zhou W, Zhu M, Liu Y, Zhao Z, Guo J (2002) Elastic and electrical properties of serpentinite dehydration at high temperature and high pressure. J Phys Condens Matter 14:11359–11363

Xu Y, Shankland TJ (1999) Electrical conductivity of orthopyroxene and its high pressure phases. Geophys Res Lett 26:2645–2648

Xu Y, Poe BT, Shankland TJ, Rubie DC (1998) Electrical conductivity of olivine, wadsleyite, and ringwoodite under upper-mantle conditions. Science 280:1415–1418

Xu Y, Shankland TJ, Duba AG (2000a) Pressure effect on electrical conductivity of mantle olivine. Phys Earth Planet Inter 118:149–161

Xu Y, Shankland TJ, Poe BT (2000b) Laboratory-based electrical conductivity in the Earth's mantle. J Geophys Res 105:27865–27875

Yang X, Keppler H, McCammon C, Ni H, Xia Q, Fan Q (2011a) Effect of water on the electrical conductivity of lower crustal clinopyroxene. J Geophys Res 116:B04208. doi:10.1029/2010JB008010

Yang X, Keppler H, McCammon C, Ni H (2011b) Electrical conductivity of orthopyroxene and plagioclase in the lower crust. Contrib Miner Petrol 161. doi:10.1007/s00410-011-0657-9

Zhang B, Katsura T, Shatskiy A, Matsuzaki T, Wu X (2006) Electrical conductivity of $FeTiO_3$ ilmenite at high temperature and high pressure. Phys Rev B 73:134014. doi:10.113/PhysRevB.73.134104

Zhang B, Wu X, Xu J, Katsura T, Yoshino T (2010) Electrical conductivity of enstatite up to 20 GPa and 1600 K. Chinese J Geophys 53:760–764